

## Supplementary Materials

Dexamethasone Increases Cisplatin-Loaded Nanocarrier Delivery and Efficacy in Metastatic Breast Cancer by Normalizing the Tumor Microenvironment

John D. Martin<sup>1</sup>, Myrofora Panagi<sup>2</sup>, Chenyu Wang<sup>3</sup>, Thahomina T. Khan<sup>1</sup>, Margaret R. Martin<sup>1</sup>, Chrysovalantis Voutouri<sup>2</sup>, Kazuko Toh<sup>4</sup>, Panagiotis Papageorgis<sup>2,5</sup>, Fotios Mpekris<sup>2</sup>, Christiana Polydorou<sup>2</sup>, Genichiro Ishii<sup>6</sup>, Shinichiro Takahashi<sup>7</sup>, Naoto Gotohda<sup>7</sup>, Toshiyuki Suzuki<sup>7</sup>, Matthew E. Wilhelm<sup>3</sup>, Vinicio Alejandro Melo<sup>4</sup>, Sabina Quader<sup>4</sup>, Jumpei Norimatsu<sup>1</sup>, Ryan M. Lanning<sup>8</sup>, Motohiro Kojima<sup>6</sup>, Matthew David Stuber<sup>3</sup>, Triantafyllos Stylianopoulos<sup>2</sup>, Kazunori Kataoka<sup>4,9\*</sup>, and Horacio Cabral<sup>1\*</sup>

Affiliations:

<sup>1</sup> *Department of Bioengineering, Graduate School of Engineering, The University of Tokyo, Bunkyo, Tokyo, 113-8656, Japan.*

<sup>2</sup> *Cancer Biophysics Laboratory, Department of Mechanical and Manufacturing Engineering, University of Cyprus, Nicosia, 1678, Cyprus.*

<sup>3</sup> *Process Systems and Operations Research Laboratory, Department of Chemical and Biomolecular Engineering, University of Connecticut, Storrs, Connecticut, 06269, USA.*

<sup>4</sup> *Innovation Center of NanoMedicine, Kawasaki Institute of Industrial Promotion, Kawasaki, Kanagawa, 210-0821, Japan.*

<sup>5</sup> *Department of Life Sciences, Program in Biological Sciences, European University Cyprus, Nicosia, 1516, Cyprus.*

<sup>6</sup> *Exploratory Oncology Research & Clinical Trial Center, National Cancer Center, Kashiwa, Chiba, 277-8577, Japan.*

<sup>7</sup> *Department of Hepatobiliary-Pancreatic Surgery, National Cancer Center Hospital East, Kashiwa, Chiba, 277-8577, Japan.*

<sup>8</sup> *Department of Radiation Oncology, School of Medicine, University of Colorado, Aurora, Colorado, 80045, USA.*

<sup>9</sup> *Institute for Future Initiatives, The University of Tokyo, Bunkyo, Tokyo, 113-0033, Japan.*

\* *Correspondence to: kataoka@ifi.t.u-tokyo.ac.jp (KK), horacio@bmw.t.u-tokyo.ac.jp (HC)*

## Mathematical Model

Equations and assumptions: We used a 1-dimensional spherical tumor transport model. We assumed spatial independence for physiological parameters, which does not account for the heterogeneity of the tumor microenvironment (TME). Besides not considering vessels, cells and extracellular matrix (ECM) explicitly, we also assume a lack of lymphatics and nanocarrier (NC) binding. Lymphatics within tumors are largely non-functional. NCs are PEGylated to limit cellular interaction. Given our bolus injection mode of administration of probe and NC, we assume the source of fluid and NC is distributed continuously over the spatial domain and NC concentration decays exponentially.

The interstitial fluid transport follows Darcy's law and we assume axisymmetric flow:

$$\mathbf{u} = -K\nabla p$$

where  $\mathbf{u}$  is the interstitial fluid velocity (cm/s),  $K$  is the hydraulic conductivity of tumor interstitium (cm<sup>2</sup>/mm Hg-sec),  $p$  is the interstitial fluid pressure (IFP) in mmHg.

We substituted the above equation into the fluid continuity equation to obtain the steady-state fluid transport model:

$$\nabla^2 p = \frac{SL_p}{VK}(p - p_{ss})$$

where  $L_p$  is the hydraulic conductivity of microvascular wall (cm/mmHg-sec),  $\frac{S}{V}$  is the vascular surface area per unit volume (cm<sup>-1</sup>), and  $p_{ss}$  is the steady-state interstitial pressure where the efflux from the vessels equals to the influx (mmHg).

The boundary conditions consist of the no-flux condition at the center of the spherical tumor and fixed tissue pressure  $p_\infty$  at the tumor edge ( $r=R$ ):

$$\begin{aligned}\nabla p|_{r=0} &= 0 \\ p|_{r=R} &= p_\infty\end{aligned}$$

Solute transport follows the dynamic convection-diffusion equation below.

$$\frac{\partial C}{\partial t} + \nabla \cdot (\mathbf{u}C) = \nabla \cdot (D\nabla C) + \phi_s$$

where  $C$  is the concentration of the NC in the interstitium of the tumor (g/ml),  $D$  is the diffusion coefficient (cm<sup>2</sup>/sec), and  $\phi_s$  is the distributed source term based on the pore model for transcapillary exchange:

$$\phi_s = L_p \frac{S}{V} (p_v - p)(1 - \sigma)C_v + P \frac{S}{V} (C_v - C) \frac{Pe}{e^{Pe} - 1}$$

where  $p_v$  is the microvascular pressure (MVP) in mmHg;  $Pe = L_p(p_v - p)(1 - \sigma)/P$  is the Peclet number representing the ratio of convective forces to diffusion forces across the vascular wall;  $\sigma$  is the solute reflection coefficient;  $P$  is the vascular permeability of the solute through the vascular wall (cm/sec); and  $C_v$  is the probe concentration in tumor vessels (g/ml). As described above, we assumed the vascular solute concentration decays exponentially with time:

$$C_v = C_o e^{-t/k_d}$$

where  $C_o$  is the initial probe concentration in the blood (g/ml), and  $k_d$  is the half-life circulation time of the probe (sec). The probe concentration satisfies the no-flux condition at the center and is continuous across the tumor periphery:

$$\begin{aligned} -D \frac{\partial C}{\partial r} \Big|_{r=0} + uC \Big|_{r=0} &= 0 \\ C \Big|_{r=R} &= C_\infty \end{aligned}$$

We followed the pore theory<sup>1</sup> to describe NC transport through the walls of vessels. Assuming the vessels to be cylindrical, we can evaluate the hydraulic conductivity of the vessels  $L_p$ , the vascular permeability  $P$ , and the solute reflection coefficient  $\sigma$  with the following three equations:

$$L_p = \frac{\gamma r_o^2}{8\mu L}$$

$$P = \frac{\gamma H D_o}{L}$$

$$\sigma = 1 - W$$

where  $\gamma$  is the fraction of the surface area occupied by pores;  $r_o$  is the pore radius (nm);  $\mu$  is the blood viscosity (mmHg-sec);  $L$  is the thickness of the vessel wall ( $\mu$ m);  $D_o$  is the diffusion coefficient of the NC in free solution at 37°C given by the Stokes-Einstein relationship;  $H$  and  $W$  are diffusive and convective hindrance factors, respectively, based on the size ratio of NC to pore<sup>1,2</sup>:

$$H = \frac{6\pi\Phi}{K_t}$$

$$W = \frac{\Phi(2-\Phi)K_s}{2K_t}$$

where  $\Phi$  is the partitioning coefficient defined as the ratio of the average intrapore concentration to that in the bulk solution at equilibrium. When the interactions between the solutes and pore wall are purely steric, the partitioning coefficient is taken as  $\Phi = (1-\lambda)^2$ , where  $\lambda$  is the ratio of particle size to the pore size.  $K_t$  and  $K_s$  factors for the convective hindrance term  $W$  are defined as follows:

$$K_t = \frac{9}{4}\pi^2\sqrt{2}(1-\lambda)^{-5/2} \left[ 1 + \sum_{k=1}^2 a_k (1-\lambda)^k \right] + \sum_{k=0}^4 a_{k+3} \lambda^k$$

$$K_s = \frac{9}{4}\pi^2\sqrt{2}(1-\lambda)^{-5/2} \left[ 1 + \sum_{k=1}^2 b_k (1-\lambda)^k \right] + \sum_{k=0}^4 b_{k+3} \lambda^k$$

The corresponding coefficients  $a_k$  and  $b_k$  are listed in Supplementary Table M1.

**Supplementary Table M1: Hydrodynamic Coefficients for the Cylindrical Pore Model**

$k$	1	2	3	4	5	6	7
$a_k$	-73/60	77293/50400	-22.5083	-5.6117	-0.3363	-1.216	1.647
$b_k$	7/60	-2227/50400	4.0180	-3.9788	-1.9215	4.392	5.006

Solution strategy: We solved the fluid and solute transport model numerically using a discretized form. First, we reformulated the model into its dimensionless form. Then, the finite difference method was used to derive the discrete form of the fluid transport model with the upwind scheme employed for discretization of the solute transport model. We solved these equations using the variable-step 4<sup>th</sup>-order Runge-Kutta method.

The experimentally measured values of effective permeability  $P_{eff}$  were used to obtain the average probe concentration profiles  $C_{avg}$  over the interstitial space – which are taken as data points for the parameter estimation problem – utilizing the following spatially-averaged conservation equation:

$$\frac{dC_{avg}}{dt} = P_{eff} \frac{S}{V} (C_v - C_{avg})$$

To formulate the parameter estimation optimization problem, we seek to minimize the sum of squared error (SSE) between the average concentration of the transport model  $C_{avg,mod}$  and data  $C_{avg,data}$  over the experimental time span:

$$\min_{\mathbf{P} \in P_{param}} \sum_{i=1}^n (C_{avg,mod}(t, \mathbf{P}) - C_{avg,data}(t))^2$$

Since we hypothesize dexamethasone affects the hydraulic conductivity of the vessel wall and the interstitial space, we chose  $L_p$  and  $K$  as the uncertain model parameters for estimation. For the other parameters, we used the literature values presented in Supplementary Table M2. Since the Peclet number can be very high at some parameter values, the problem can be very stiff. To obtain better local optimization results, we multistart *fmincon* in MATLAB (The MathWorks) with the interior-point solver and pick the results with the lowest objective function values. This approach, along with local analysis, provide a high-likelihood of obtaining near-global optimal results for the two-variable problem.

### Supplementary Table M2: Physiological Parameter Values for Use in the Model

Parameter	Definition	Value	Reference
$S/V$ (cm <sup>-1</sup> )	Vascular density	200	3
$D$ (cm <sup>2</sup> /sec)	Diffusion coefficient	2e-7 (13 nm); 1.375e-7 (32 nm)	4
$p_v$ (mm Hg)	Vascular pressure	25	5
$k_d$ (min)	Blood circulation time	1480 (13 nm); 1278 (32nm)	6
$\mu$ (mm Hg-sec)	Blood viscosity	3e-5	7
$L$ ( $\mu$ m)	Vessel wall thickness	5	8
$\gamma$	Fraction of pore area	1e-3	9

Results and analysis: The local optima are shown in Supplementary Table M3.

The model predictions of vessel wall pore diameter and interstitial hydraulic conductivity produced from effective permeability measurements are consistent with our other experimental data. Specifically, our model predicts both doses of dexamethasone raise the interstitial hydraulic conductivity to a similar level. This is expected based on the similar effects of both doses on collagen I (Fig. 2C) and hyaluronan (Fig. 2D) levels

measured histologically. Furthermore, our model predicts that, while 3 mg/kg dexamethasone reduces vessel pore diameter by only 10%, 30 mg/kg dexamethasone reduces vessel pore size by 45%. This model prediction is consistent with the notion that the higher dose produces a stronger anti-angiogenic effect. Specifically, we observe more vessel pruning (Fig. 1D,E) and a distribution of vessel diameters skewing towards diameters (Supplementary Fig. S3,4) with 30 mg/kg dexamethasone treatment.

**Supplementary Table M3: Local Optimums for Parameter Estimation Results**

Results	70 kDa rhodamine			500 kDa FITC		
	Control	3 mg/kg	30 mg/kg	Control	3 mg/kg	30 mg/kg
$P_{eff}$ (cm/sec)	9.60e-7	4.61e-6	2.80e-6	8.18e-7	4.30e-6	1.62e-6
$L_p$ (cm/mm Hg-sec)	1.04e-6	1.49e-6	3.50e-7	8.67e-7	7.17e-7	2.81e-7
K (cm <sup>2</sup> /mm Hg-sec)	2.33e-7	8.57e-7	1.56e-6	2.97e-7	1.63e-6	1.68e-6
IFP (mm Hg)	24.01	23.46	20.30	23.80	21.85	19.32
Pore diameter (nm)	223	267	130	204	185	116

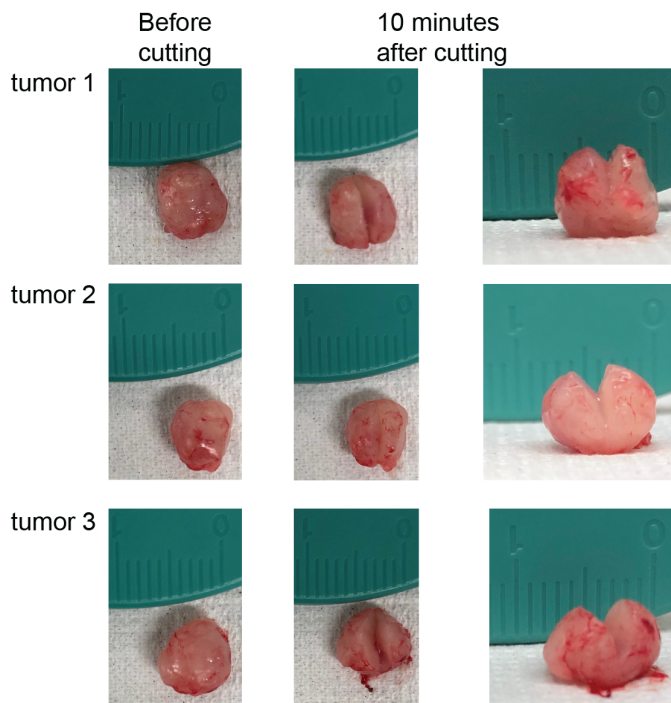
## Supplementary Figures and Tables

**Supplementary Table 1** – Dose schedule (timing in the header) of the current study in mice (top row) compared to the doses of clinical trials of CDDP/m (NCT02043288) converted from human to mouse doses by body surface area (bottom row). The total dose of dexamethasone is in the right column.

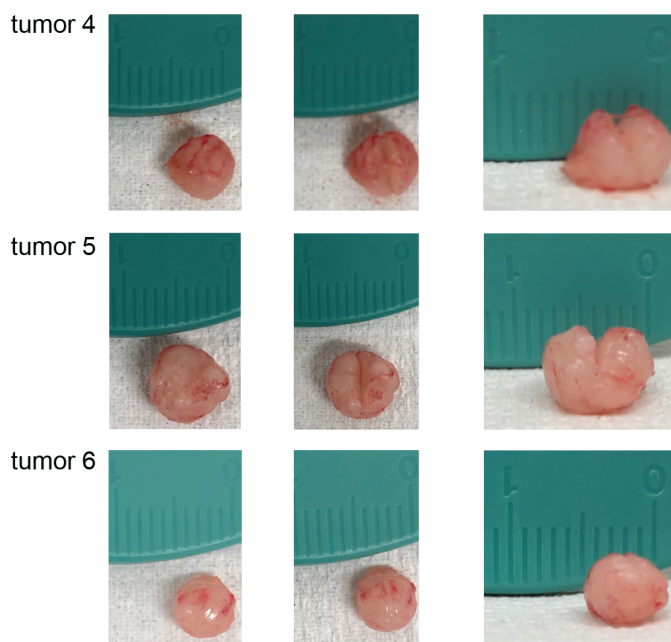
Time relative to CDDP/m	-72	-48	-24	-12	-6	0	12	24	36	48	Total dose
Current study dose [mg/kg]	3	3	3			3		*			12
CDDP/m (NC-6004) trial dose equivalent in mice [mg/kg]				4.11	4.11		0.82	0.82	0.82	0.82	11.5

\*If another cycle is initiated, 3mg/kg would be administered at this time to begin the next cycle.

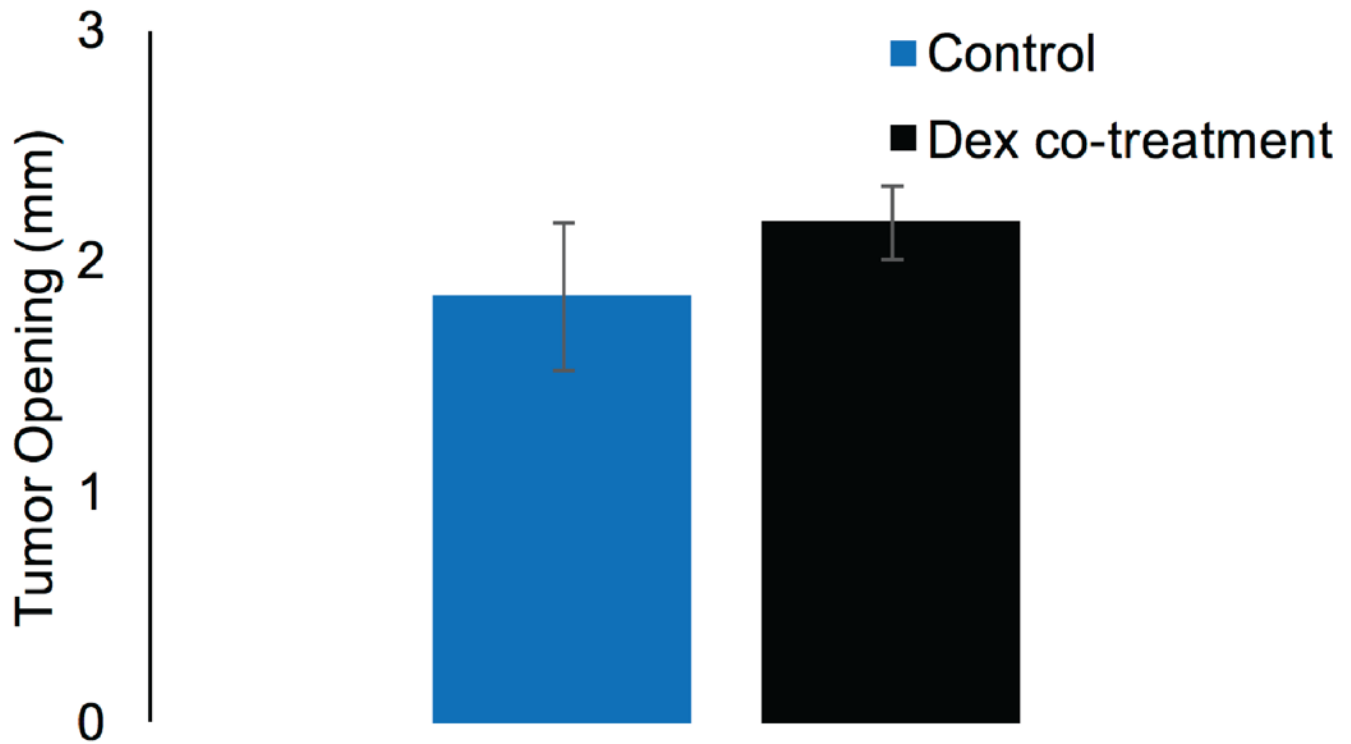
## A Control



## B Dexamethasone

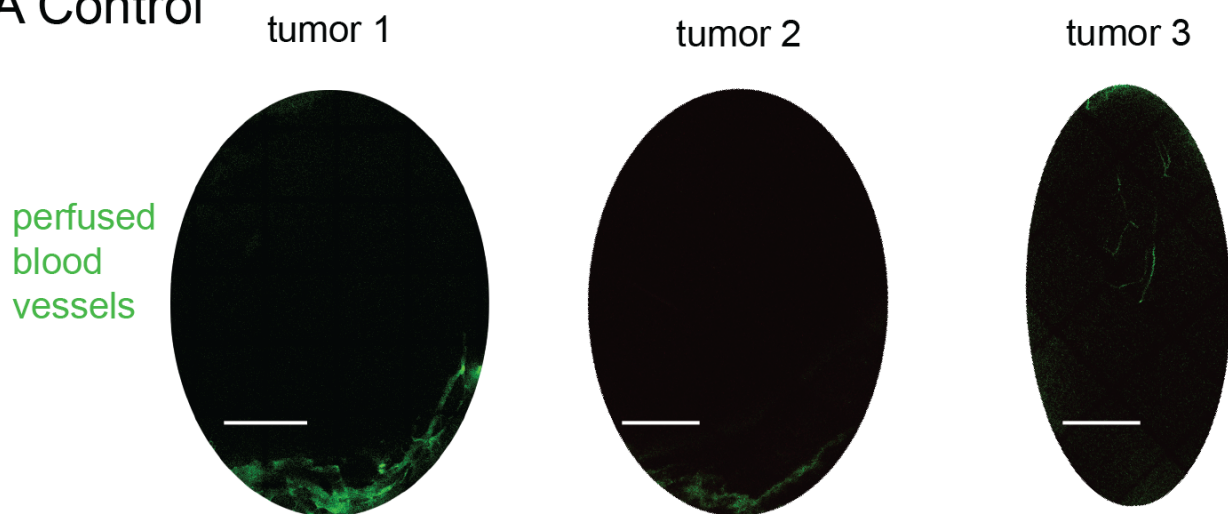


**Supplementary Figure S1. Tumor opening assay.** (A-B) Representative images of the tumor opening assay of 4T1 tumors from control (A) and 3mg/kg dexamethasone (B) treated mice. (Left column) Overhead images of the tumors before cutting. (Center column) Overhead images of the tumors after cutting. (Right column) *En face* images of the tumors after cutting. The tumor opening is the distance the tumor opens ten minutes after cutting. The larger the opening, the higher the solid stress in the tissues. Ruler scale in centimeters. These images were collected for representation and this data was not used in quantitation in Figure 2F.

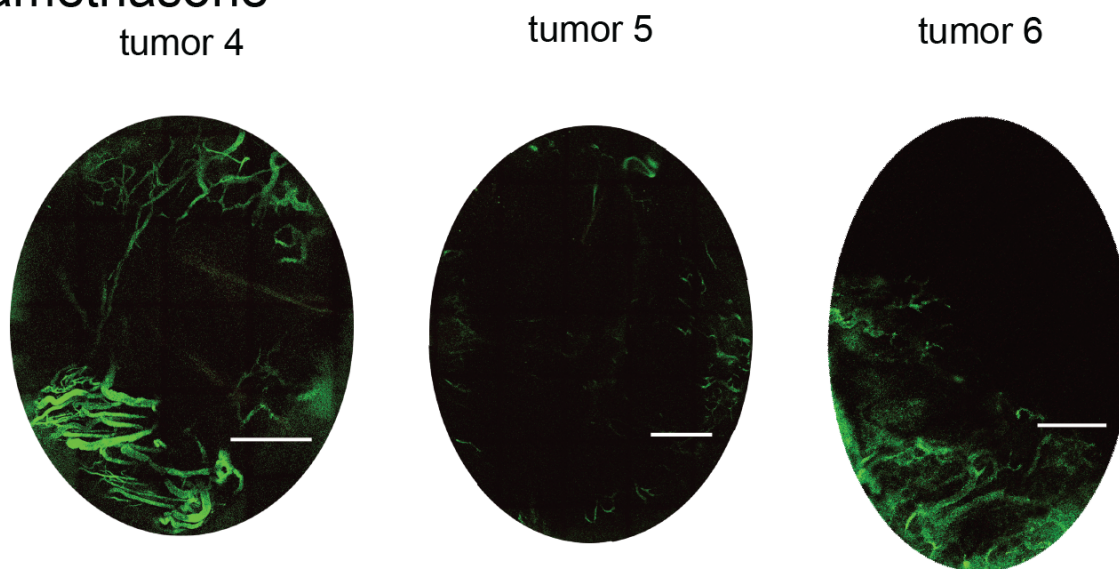


**Supplementary Figure S2. Dexamethasone co-treatment does not affect solid stress.** Quantification of the tumor opening distance, which is a measure of solid stress levels of 4T1 tumors excised from control mice (blue bar) or mice treated with 3 mg/kg dexamethasone 2 h before tumor excision and measurement (black bar,  $N = 3$  mice per group).

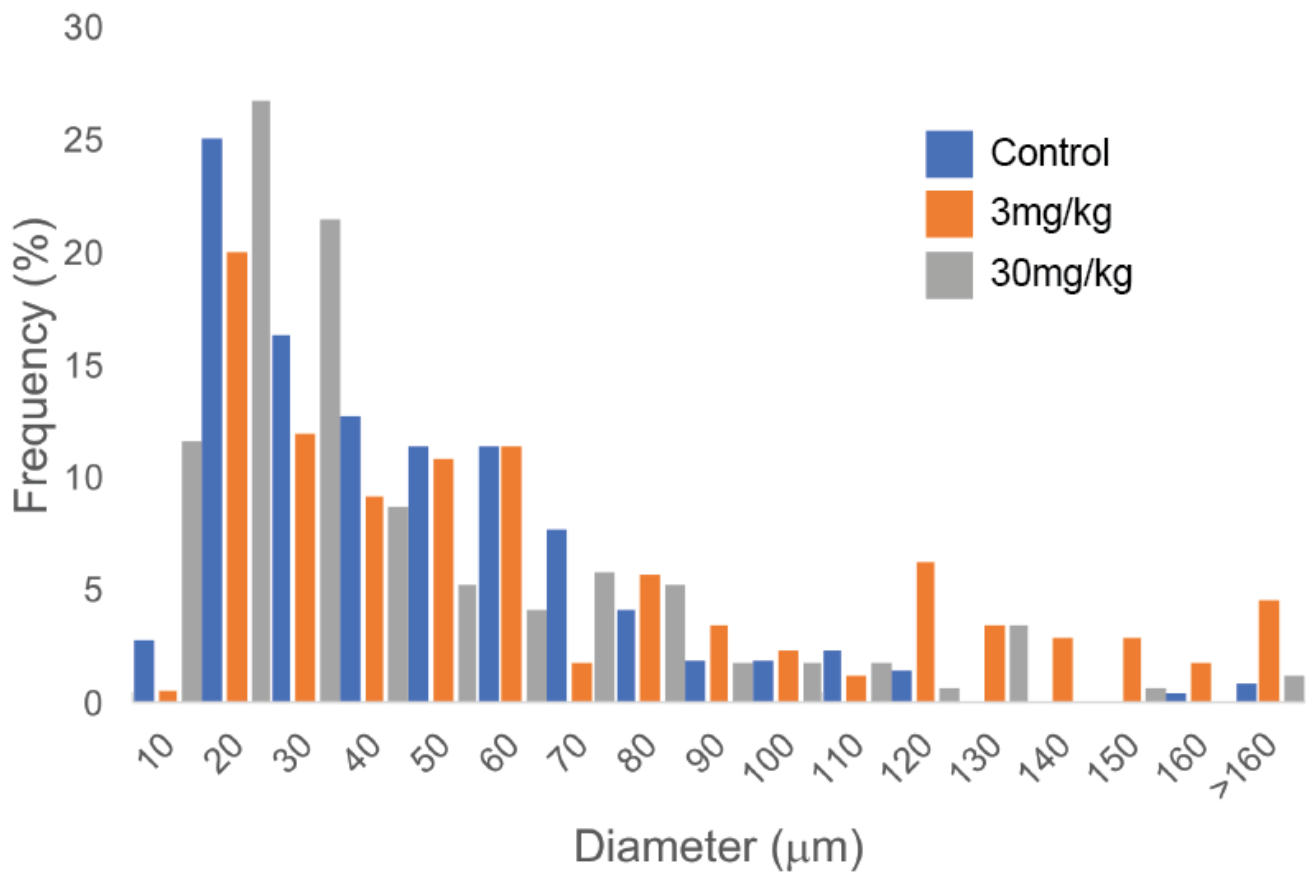
## A Control



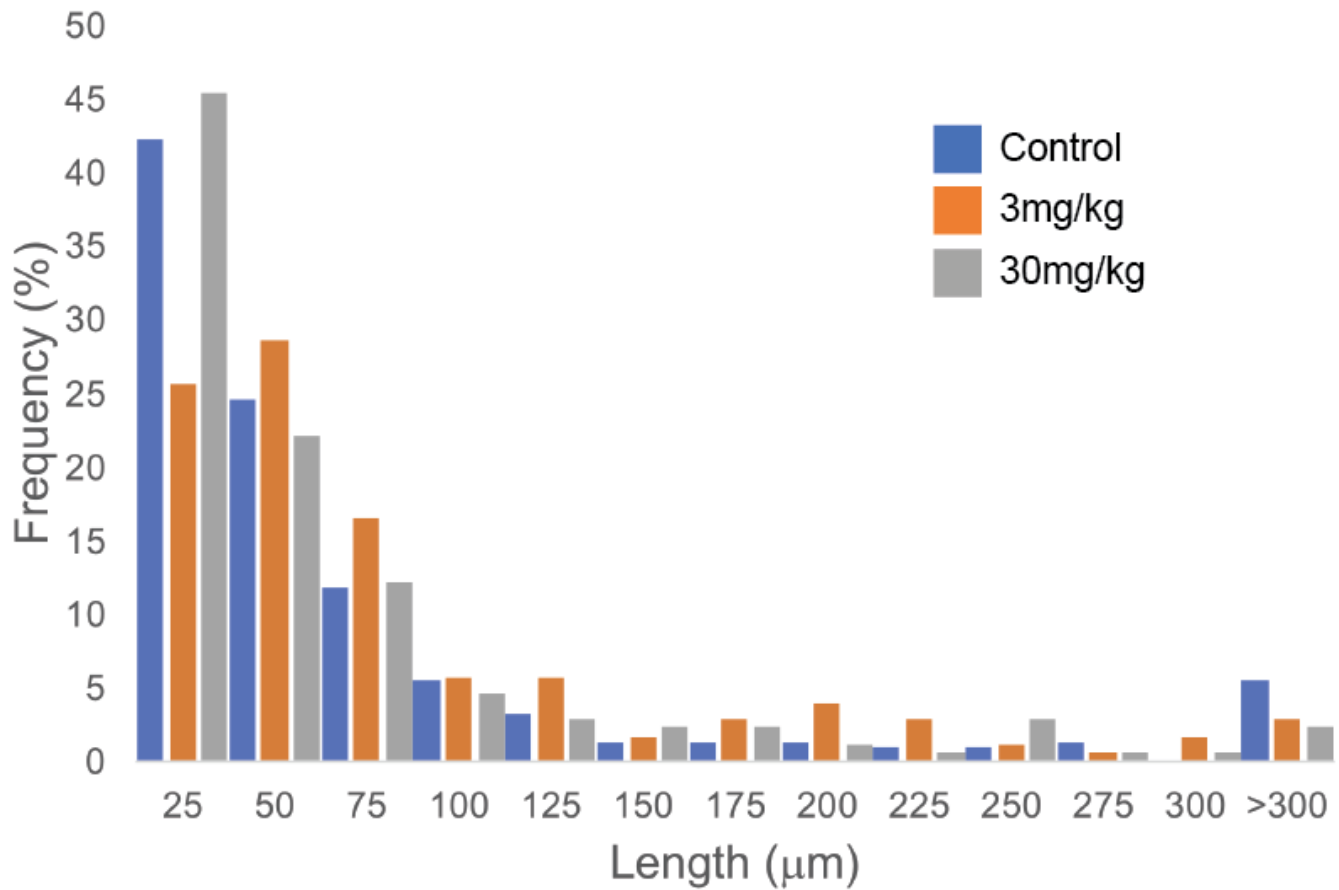
## B Dexamethasone



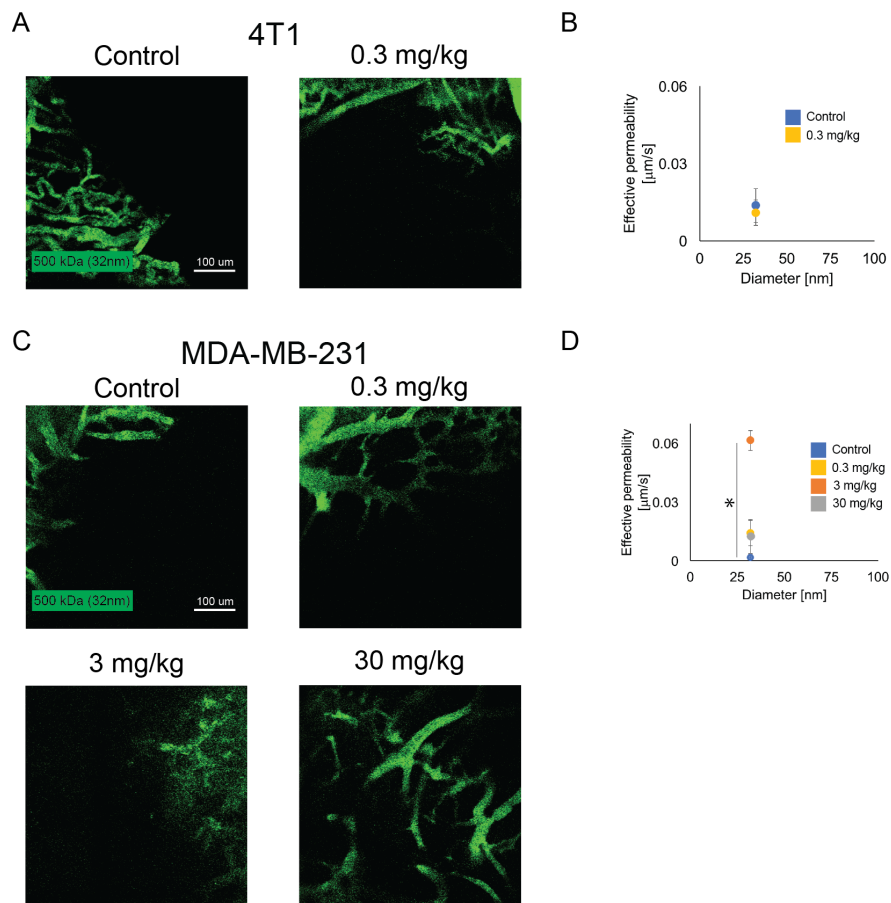
**Supplementary Figure S3. Dexamethasone affects tumor vessel function.** (A-B) Representative intravital microscopy images of perfused tumor vessels (green) of 4T1 tumors from control (A) and 3 mg/kg dexamethasone (B) treated mice. Scale bars = 600  $\mu$ m.



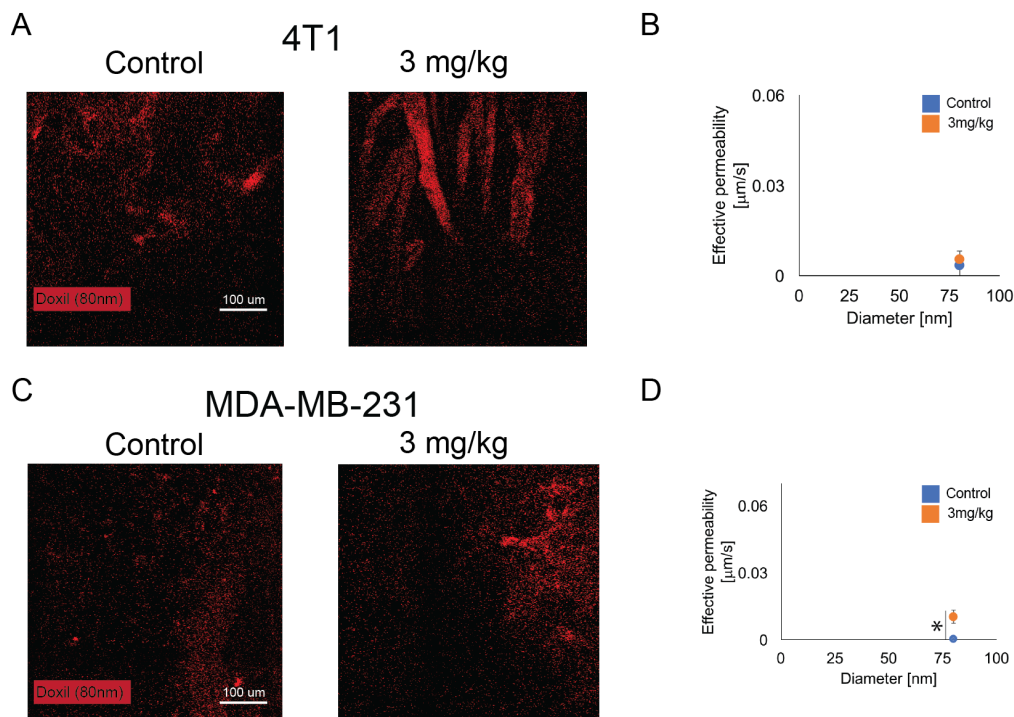
**Supplementary Figure S4. Dexamethasone normalizes the diameter of vessels.** Histograms of vessel diameters indicate a larger proportion of wider vessels with 3 mg/kg dexamethasone treatment ( $N = 3$ ,  $n = 175$ - $220$  vessels per group).



**Supplementary Figure S5. Dexamethasone normalizes the length of vessels.** Histograms of perfused vessel lengths from intravital microscopy indicate a larger proportion of longer vessels with 3 mg/kg dexamethasone treatment ( $N = 3$  mice,  $n = 175$ - $220$  vessels per group).

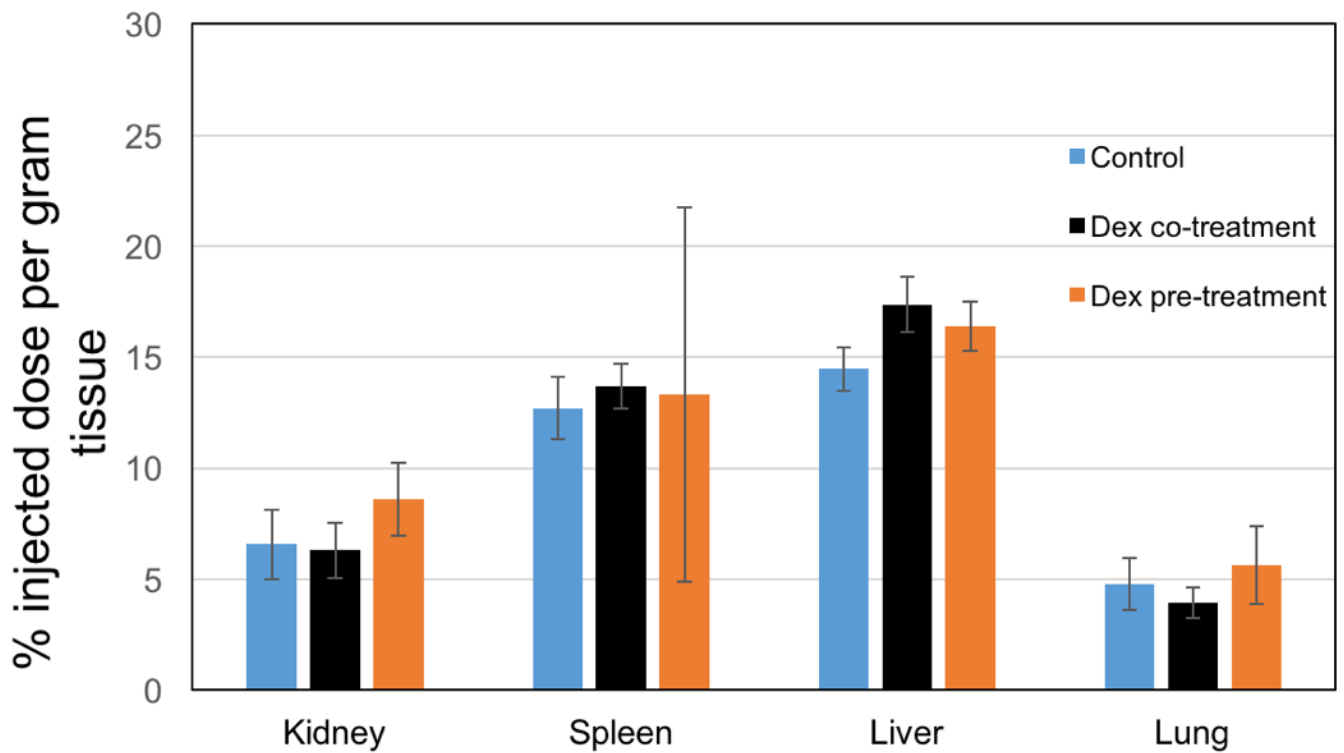


**Supplementary Figure S6. Transvascular transport of nanocarriers after treatment of dexamethasone at various doses.** Transvascular transport in 4T1 (**A, B**) and MDA-MB-231 (**C, D**) breast cancers, with (**A,C**) representative confocal intravital microscopy images of tumors. (**A**) 4T1 bearing mice were treated 4 days daily with (**left panel**) control or (**right panel**) 0.3 mg/kg dexamethasone, and the representative images show the distribution 20 min after injection of 500 kDa (32 nm, green) fluorescent dextrans. (**B**) Quantification of effective permeabilities, which is a measure of the rate that dextrans are transporting out of vessels and penetrating after treatment with 0.3 mg/kg dexamethasone (yellow circles) and control (blue circles) in mice bearing 4T1 breast tumors ( $N = 3$ ). (**C**) MDA-MB-231 bearing mice were treated 4 days daily with (**top left panel**) control, (**top right panel**) 0.3 mg/kg, (**bottom left panel**) 3 mg/kg or (**bottom right panel**) 30 mg/kg dexamethasone, and the representative images show the distribution 20 min after injection of 500 kDa (32 nm, green) fluorescent dextrans. (**D**) Quantification of effective permeabilities after treatment of 4 days daily dexamethasone at 0.3 mg/kg (yellow circles), 3 mg/kg (orange circles), 30 mg/kg (gray circles) and control (blue circles) doses in mice bearing MDA-MB-231 breast tumors ( $N = 3$ ). Data expressed as mean  $\pm$  standard error of the mean (\*,  $P < 0.05$ ).

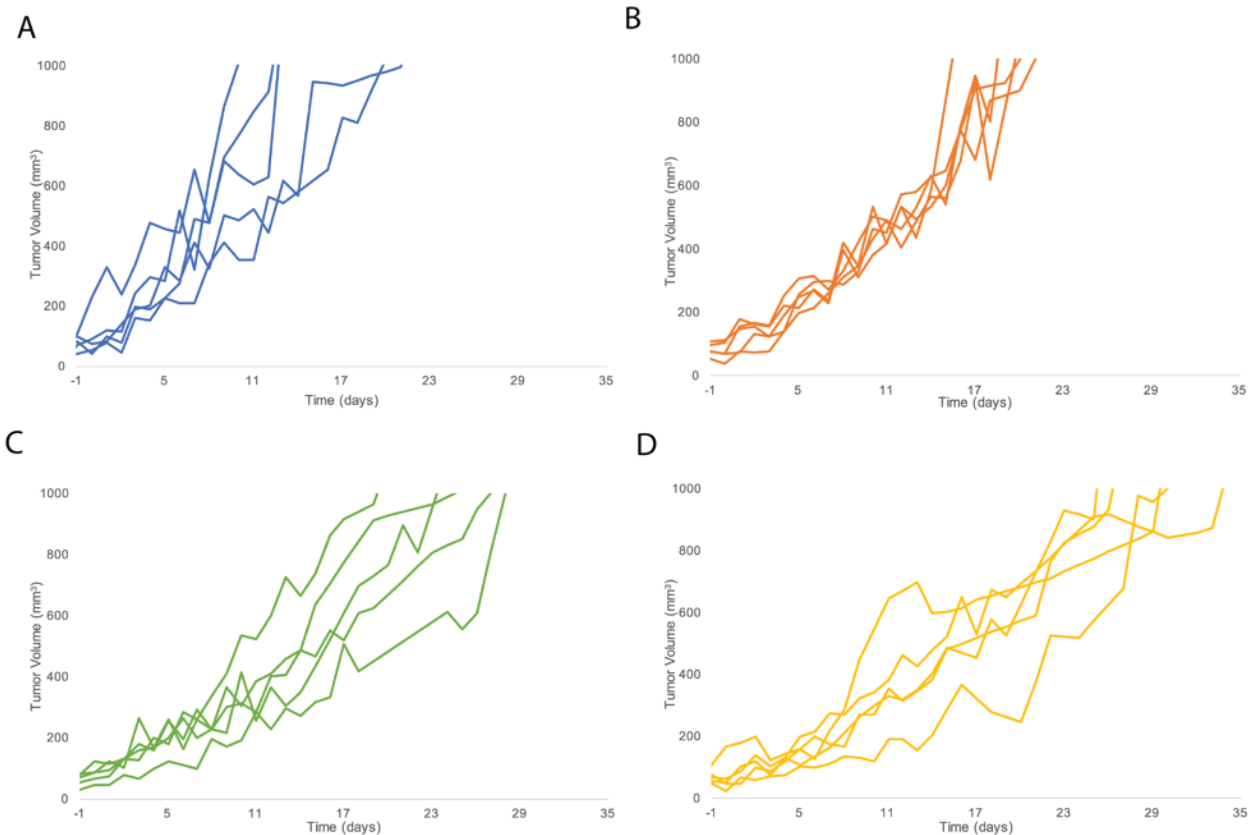


**Supplementary Figure S7. Transvascular transport of Doxil after treatment of dexamethasone.**

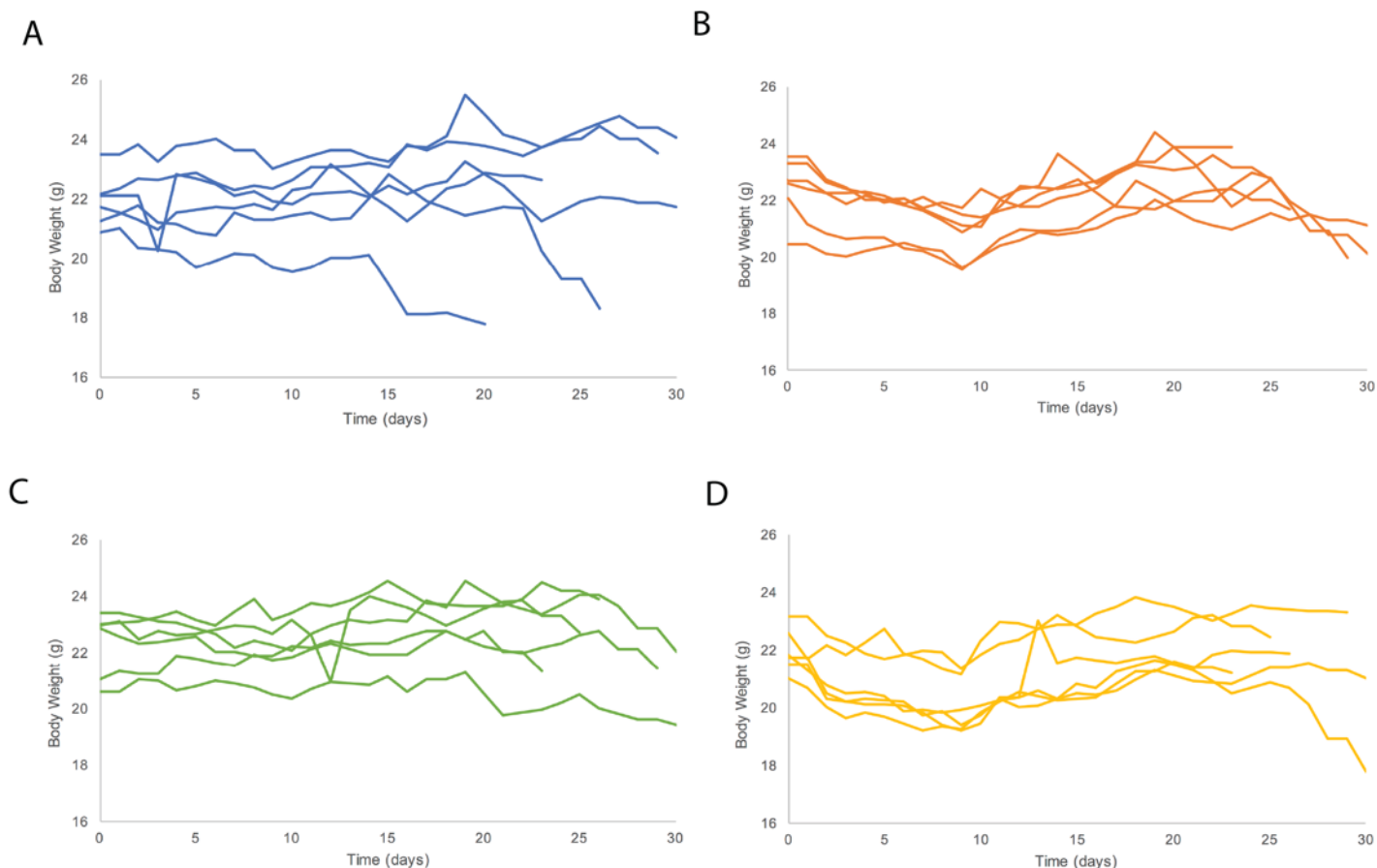
Transvascular transport in 4T1 (**A, B**) and MDA-MB-231 (**C, D**) breast cancers, with (**A,C**) representative confocal intravital microscopy images of tumors. (**A**) 4T1 bearing mice were treated with (**left panel**) control or (**right panel**) 3 mg/kg dexamethasone, and the images show the distribution 20 min after injection of Doxil (80 nm, red). (**B**) Quantification of 4T1 effective permeabilities, which is a measure of the rate that Doxil is transporting out of vessels and penetrating after treatment of either 4 days daily dexamethasone 3 mg/kg (orange circles) or control (blue circles,  $N = 3$ ). (**C**) MDA-MB-231 bearing mice were treated with (**left panel**) control or (**right panel**) 3 mg/kg dexamethasone, and the images show the distribution 20 min after injection of Doxil (80 nm, red). (**D**) Quantification of MDA-MB-231 effective permeabilities after treatment of either 4 days daily dexamethasone 3 mg/kg (orange circles) or control (blue circles,  $N = 3$ ). Data expressed as mean  $\pm$  standard error of the mean (\*,  $P < 0.05$ ).



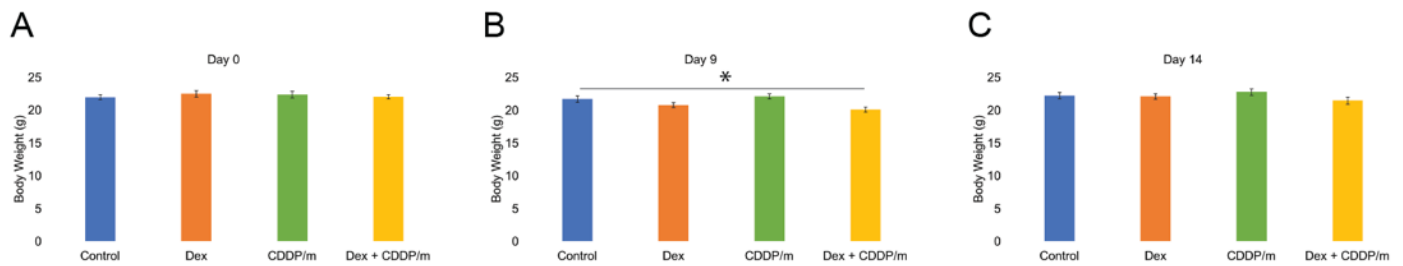
**Supplementary Figure S8. Tissue distribution of CDDP/m with and without dexamethasone in major organs 24 h after CDDP/m administration.** CDDP/m (5.5 mg/kg) was administered to 4T1 bearing mice ( $N = 6$  per group) 2 h after the final dose of daily 3 mg/kg dexamethasone pre-treatment (orange bars) or a single dose of 3 mg/kg dexamethasone as a “co-treatment” (black bars). All data expressed as mean  $\pm$  standard error of the mean.



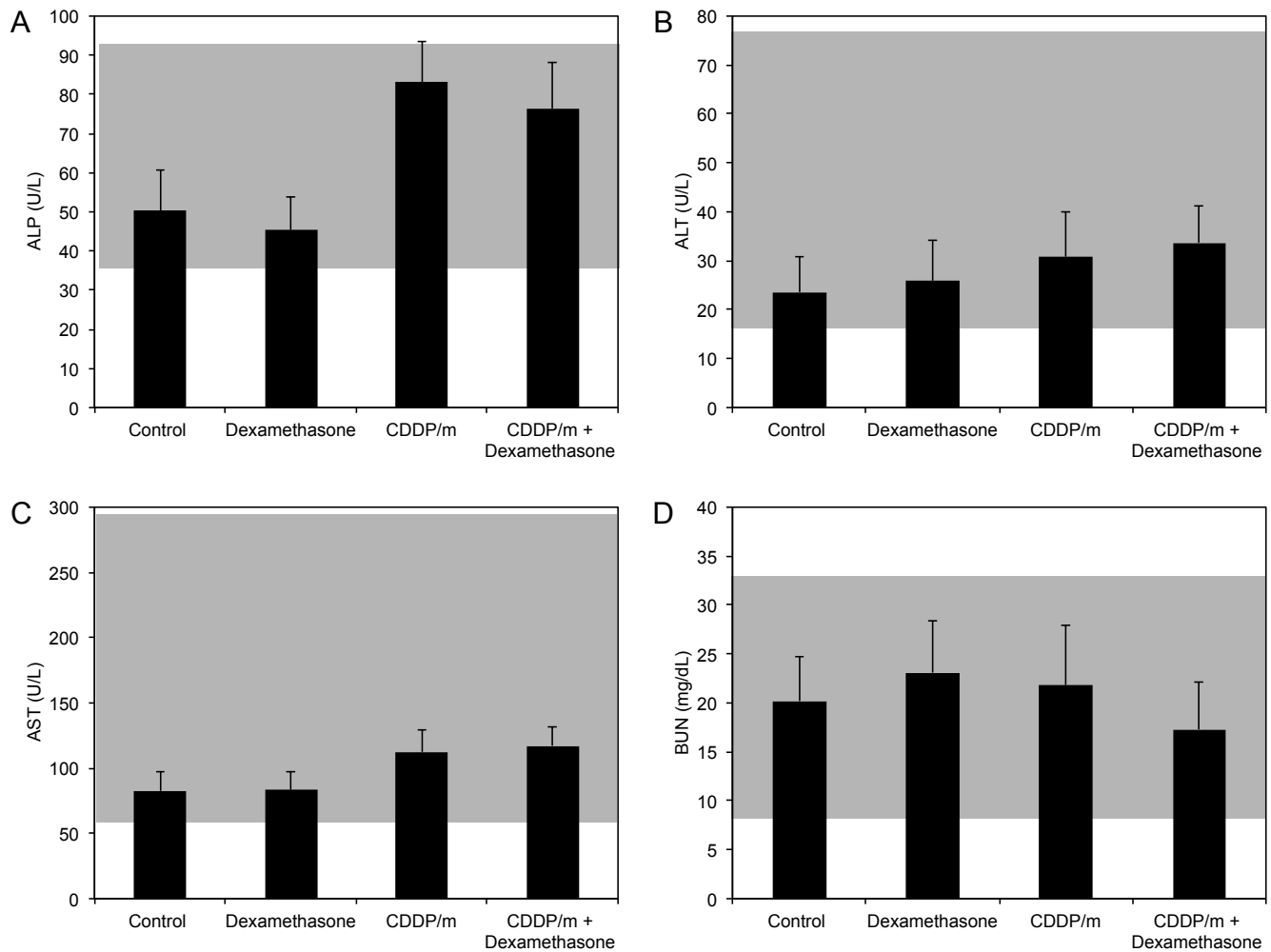
**Supplementary Figure S9. Dexamethasone increases the efficacy of 30nm CDDP/m in primary breast cancer.** (A-D) Tumor growth delay study in a syngeneic, orthotopic 4T1 breast tumor model treated with dexamethasone, CDDP/m, or the combination ( $N = 6$ ). (A) Saline (control) treated mice tumors (blue) took an average of 3.2 days for the tumor volume to double and 17 days to reach 1000 cubic millimeters. (B) Dexamethasone treated mice tumors (orange) took 3.0 days for the tumor volume to double and 20 days to reach 1000 cubic millimeters. (C) CDDP/m treated mice tumors (green) took 3.8 days for the tumor volume to double and 24 days to reach 1000 cubic millimeters. (D) Dexamethasone and CDDP/m combination treated mice tumors (yellow) took 5.0 days for the tumor volume to double and 28 days to reach 1000 cubic millimeters.



**Supplementary Figure S10. Mouse body weight during the dexamethasone and 30nm CDDP/m tumor growth study in primary breast cancer. (A-D)** Individual body weights measured during the tumor growth delay study in a syngeneic, orthotopic 4T1 breast tumor model treated with dexamethasone, CDDP/m, or the combination ( $N = 6$ ). **(A)** Saline (control) treated mice (blue) lost weight earliest before morbidity. **(B)** Dexamethasone treated mice tumors (orange) seemed to lose weight after the initial period of treatment and associated with morbidity towards the end of the study. **(C)** CDDP/m treated mice tumors (green) seemed to lose weight only associated with morbidity towards the end of the study. **(D)** Dexamethasone and CDDP/m combination treated mice tumors (yellow) seemed to lose weight after the initial period of treatment but mostly retained their weight towards the end of the study.



**Supplementary Figure S11. The combination of dexamethasone and CDDP/m induces limited weight loss immediately following the treatment regimen. (A-C)** Average mouse weights from the tumor growth delay study at various days in syngeneic, orthotopic 4T1 breast tumors treated with dexamethasone, CDDP/m, or the combination ( $N = 6$ ). **(A)** All treatment groups started with the same body weight pre-treatment. **(B)** Combination treated mice had significantly lower body weight than the controls on the day 9, which was the conclusion of therapy ( $P = 0.03$ ). **(C)** Combination treated mice did not have different weights than the control on day 14, which was 5 days after the conclusion of treatment. All data expressed as mean  $\pm$  standard error of the mean (\*,  $P < 0.05$ ).



**Supplementary Figure S12. Serum biochemistry of the mice after the treatments.** Serum was collected from all mice after the final mouse reached the endpoint of the primary tumor efficacy study and serum biochemistry was assessed (n = 4). **(A-D)** Averages of serum biochemistry within each treatment group. **(A)** ALP, alkaline phosphatase. **(B)** ALT, alanine aminotransferase; **(C)** AST, aspartate aminotransferase. **(D)** BUN, blood urine nitrogen. Gray areas indicate the normal ranges for the markers. All data expressed as mean  $\pm$  standard error of the mean.

## Supplementary References

1. Bungay, P. M.; Brenner, H., The Motion of a Closely-Fitting Sphere in a Fluid-Filled Tube. *Int. J. Multiphase Flow* **1973**, *1*, 25-56.
2. Deen, W., Hindered Transport of Large Molecules in Liquid - Filled Pores. *AIChE J.* **1987**, *33*, 1409-1425.
3. Yuan, F.; Salehi, H. A.; Boucher, Y.; Vasthare, U. S.; Tuma, R. F.; Jain, R. K., Vascular Permeability and Microcirculation of Gliomas and Mammary Carcinomas Transplanted in Rat and Mouse Cranial Windows. *Cancer Res* **1994**, *54*, 4564-4568.
4. Pluen, A.; Boucher, Y.; Ramanujan, S.; McKee, T. D.; Gohongi, T.; di Tomaso, E.; Brown, E. B.; Izumi, Y.; Campbell, R. B.; Berk, D. A.; Jain, R. K., Role of Tumor-Host Interactions in Interstitial Diffusion of Macromolecules: Cranial Vs. Subcutaneous Tumors. *Proc. Natl. Acad. Sci. U. S. A.* **2001**, *98*, 4628-4633.
5. Boucher, Y.; Jain, R. K., Microvascular Pressure Is the Principal Driving Force for Interstitial Hypertension in Solid Tumors: Implications for Vascular Collapse. *Cancer Res.* **1992**, *52*, 5110-5114.
6. Popović, Z.; Liu, W.; Chauhan, V. P.; Lee, J.; Wong, C.; Greytak, A. B.; Insin, N.; Nocera, D. G.; Fukumura, D.; Jain, R. K., A Nanoparticle Size Series for in Vivo Fluorescence Imaging. *Angew. Chem.* **2010**, *122*, 8831-8834.
7. Baish, J. W.; Netti, P. A.; Jain, R. K., Transmural Coupling of Fluid Flow in Microcirculatory Network and Interstitium in Tumors. *Microvasc Res* **1997**, *53*, 128-141.
8. Jain, R. K., Transport of Molecules across Tumor Vasculature. *Cancer Metastasis Rev.* **1987**, *6*, 559-593.
9. Chauhan, V. P.; Stylianopoulos, T.; Martin, J. D.; Popovic, Z.; Chen, O.; Kamoun, W. S.; Bawendi, M. G.; Fukumura, D.; Jain, R. K., Normalization of Tumour Blood Vessels Improves the Delivery of Nanomedicines in a Size-Dependent Manner. *Nat Nanotechnol* **2012**, *7*, 383-388.